Electronic Supplementary Information

Chemicals and materials

Cobalt nitrate hexahydrate ($Co(NO_3)_2 \cdot 6H_2O$), 2-methylimidazole, potassium hydroxide (KOH), sodium hydroxide (NaOH), ammonium chloride (NH_4Cl), ammonium chloride-^{15}N ($^{15}NH_4Cl$), p-aminobenzenesulfonamide, potassium sodium tartrate, potassium nitrate (KNO_3), potassium nitrate-^{15}N ($K^{15}NO_3$), mercuric iodide (HgI_2) and potassium iodide (KI) were obtained from Aladdin (Shanghai, China). hydrochloric acid (HCl) and ethanol (C_2H_5OH) were purchased from Beijing Chemical Works. DMAB was purchased from Macklin (Shanghai, China).

Characterization

The ZEISS Gemini 500 scanning electron microscopy (SEM) and a field emission scanning electron microscope (FE-SEM, HITACHI Regulus 8100) were performed to characterize the morphology of the sample. The related elemental distribution was analyzed with energy-dispersive X-ray spectroscopy (EDS, Oxford Ultim Max 65). The transmission electron microscopy (TEM) and high-resolution TEM (HRTEM) images were obtained by using a Jem2100F. ^1H NMR spectra were recorded on a superconducting-magnet NMR spectrometer (Bruker AVANCE III HD 500 MHz). X-ray diffraction (XRD) patterns were recorded with a PANalytical Empyrean powder diffractometer using Cu Kα radiation (λ= 0.1541 nm). X-ray photoelectron spectroscopy (XPS) spectra were conducted on an Thermo ESCALAB 250XI.

Determination of products

Nitrate: The obtained electrolyte was subjected to multiple dilutions. Then, 0.1 mL of HCl (1 M) and 0.01 mL of sulfamic acid solution (0.8 wt%) were introduced to the 5 mL of diluted electrolyte. After allowing it to stand for 10 min, the absorption spectrum was measured using UV-vis

spectrophotometry within the wavelength range of 300-200 nm. The calibration curve was established by employing a series of standard KNO_3 solutions.

Ammonia: To prepare Nessler's reagent, 0.7 g of KI and 1 g of HgI_2 were dispersed in 10 mL of 4 M NaOH solution and left in the dark for 24 h. Afterward, 5 mL of the diluted electrolyte, 0.1 mL of Nessler's reagent, and 0.1 mL of potassium sodium tartrate solution were mixed for 20 min. Finally, the absorption spectrum was obtained by UV-vis spectrophotometry. The calibration curve was generated by using a series of standard NH_4Cl solutions.

Isotope Labeling Experiments:

Isotope labeling experiments were carried out by using $K^{15}NO_3$ (99%) as the feed nitrogen source to confirm the source and quantify the concentration of NH_3-N. The $^{15}NH_4^+$ electrolyte was collected after electrolysis for 2 h in 1 M KOH containing 200 ppm $K^{15}NO_3$-^{15}N. The pH value of the post-electrolysis electrolyte was adjusted to 1-2 through 4 M H_2SO_4. Then, 50 μL of deuterium oxide (D_2O) was mixed with 0.5 mL of the acidified electrolyte to obtain further ^1H NMR spectra by the NMR detection.

The conversion efficiency, yield rate and faradaic efficiency (FE) were calculated by using the following formula:

$$\text{Conversion} = \Delta c_{NO_3^-} / c_0 \times 100\% \quad (1)$$

$$\text{Yield}_{NH_3} = (c_{NH_3} \times V) / (M_{NH_3} \times t \times S) \quad (2)$$

$$\text{FE} = (8F \times c \times V) / Q \quad (3)$$

Where Δc_{NO3^-} is the concentration difference of NO_3^- before and after reduction, c_0 is the initial concentration of NO_3^-, c_{NH3} is the measured NH_3 concentration, V is the electrolyte volume, t is the electrolysis time, M_{NH3} is the molar mass of NH_3, S is the geometric area of the catalyst, F is the Faraday constant (96 485 C mol^{-1}), and Q is the total charge during electrolysis.

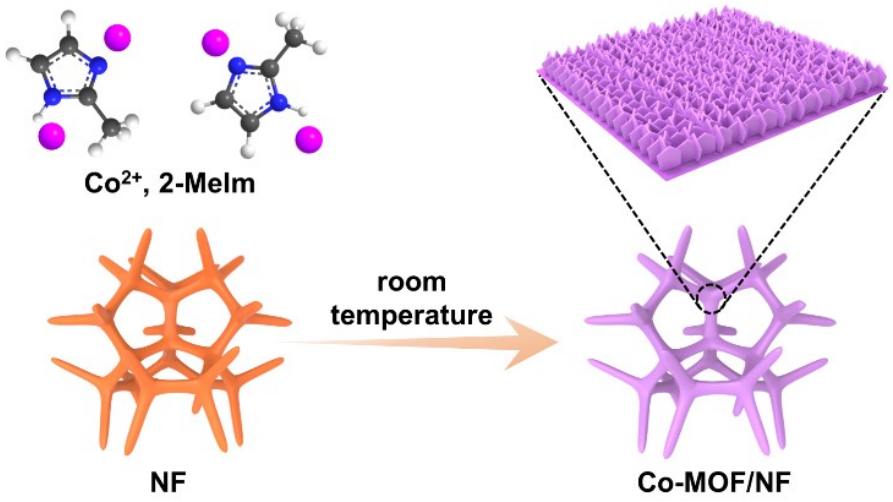

Fig. S1. Synthetic Scheme of the Co-MOF/NF.

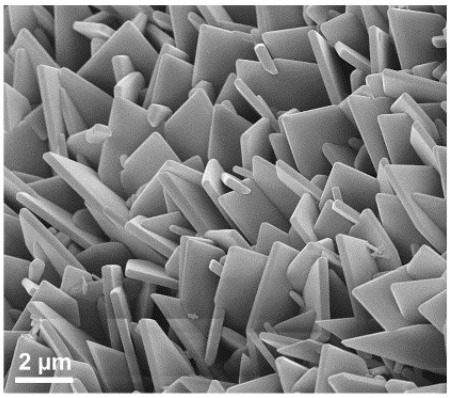

Fig. S2. SEM image of Co-MOF/NF.

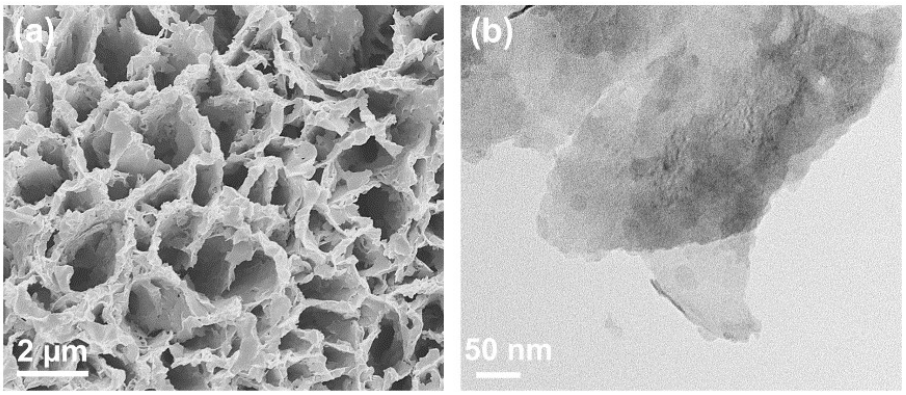

Fig. S3. (a) SEM image of DMAB-Co-MOF/NF; (b) TEM image of DMAB-Co-MOF.

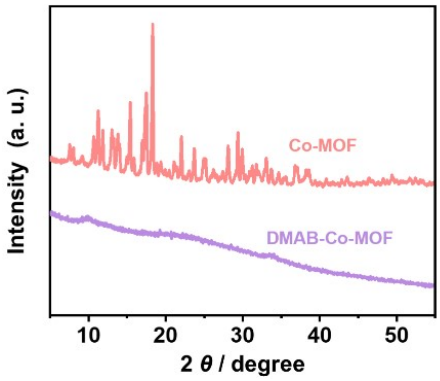

Fig. S4. XRD patterns of Co-MOF and DMAB-Co-MOF.

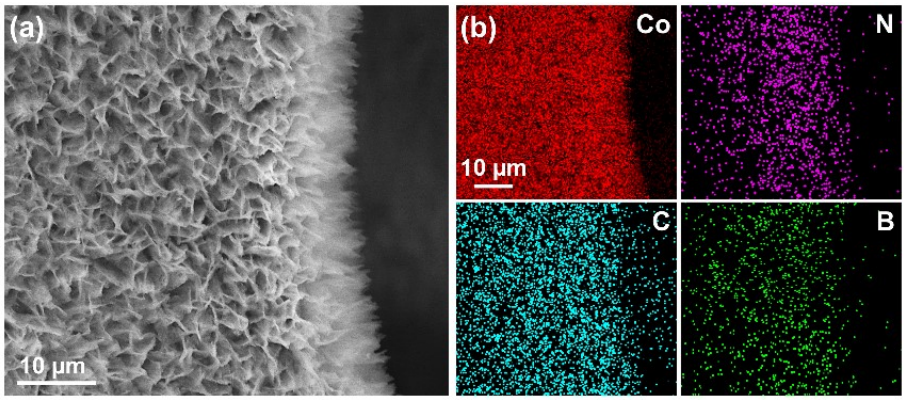

Fig. S5. (a) SEM image and (b) corresponding elemental mapping of DMAB-Co-MOF/NF.

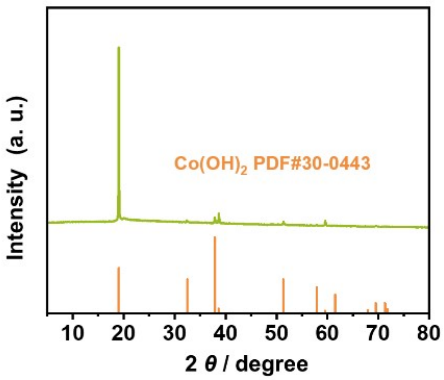

Fig. S6. XRD pattern of DMAB-Co-MOF in 1 M KOH after electrolysis.

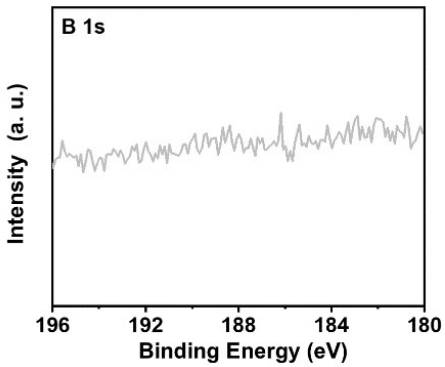

Fig. S7. B 1s XPS spectrum of $CoOOH/Co(OH)_2$.

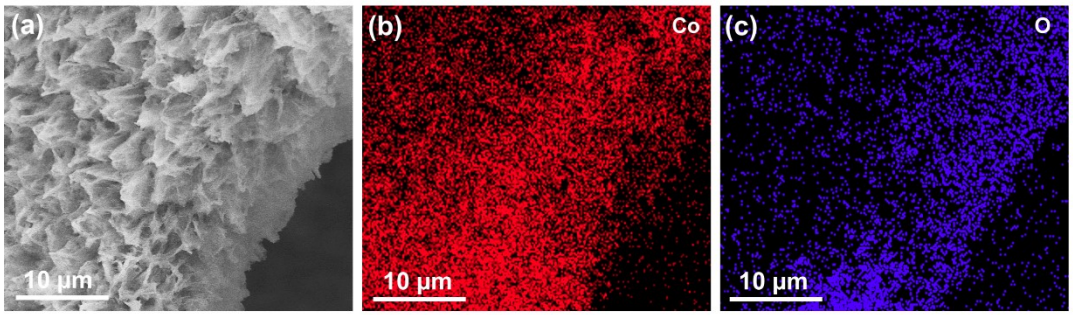

Fig. S8. (a) SEM image and (b and c) corresponding elemental mapping of $CoOOH/Co(OH)_2$/NF.

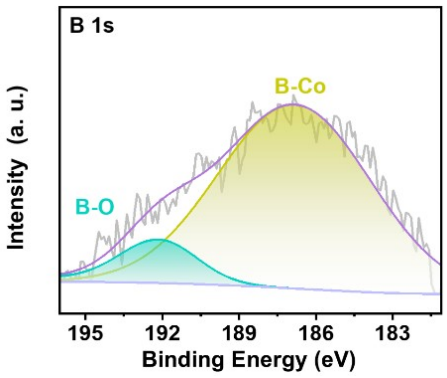

Fig. S9. B 1s XPS spectrum of B-Co-S.

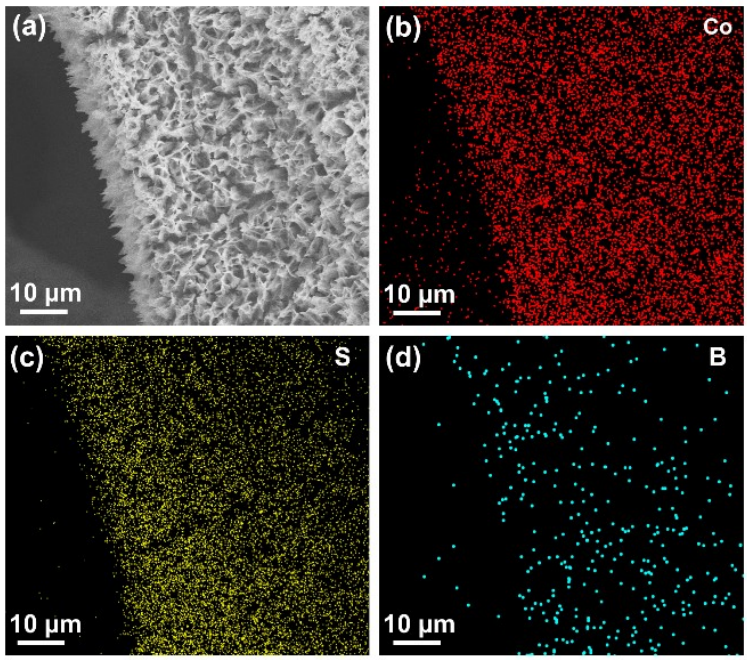

Fig. S10. (a) SEM image and (b, c and d) corresponding elemental mapping of B-Co-S/NF.

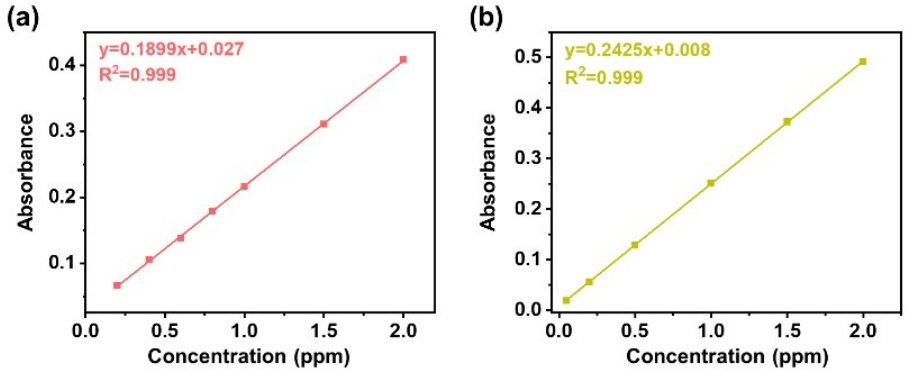

Fig. S11. Calibration curves used to estimate the concentrations of (a) NO_3^--N and (b) NH_3-N.

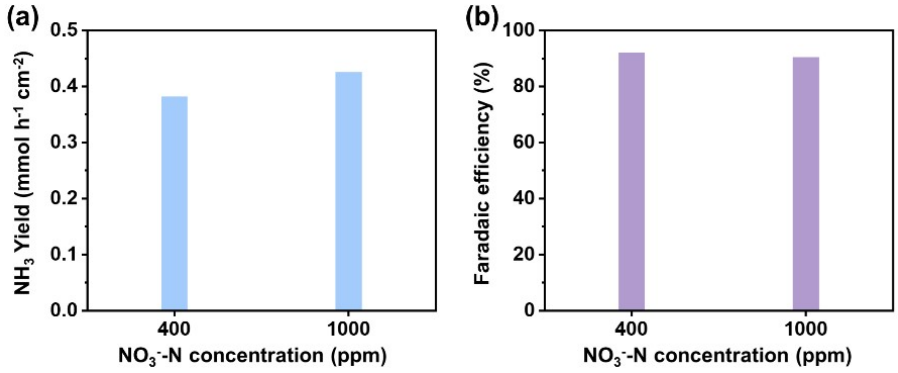

Fig. S12. (a) NH_3 yield rates and (b) NH_3 FE of $CoOOH/Co(OH)_2$/NF at different concentrations of NO_3^--N.

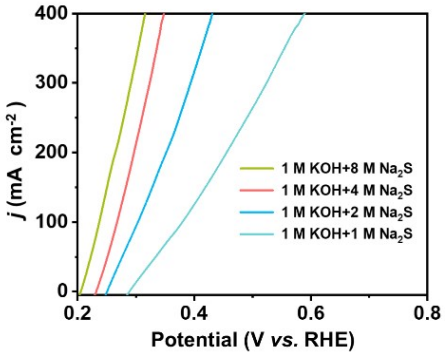

Fig. S13. LSV curves of B-Co-S/NF in different concentrations of Na_2S.

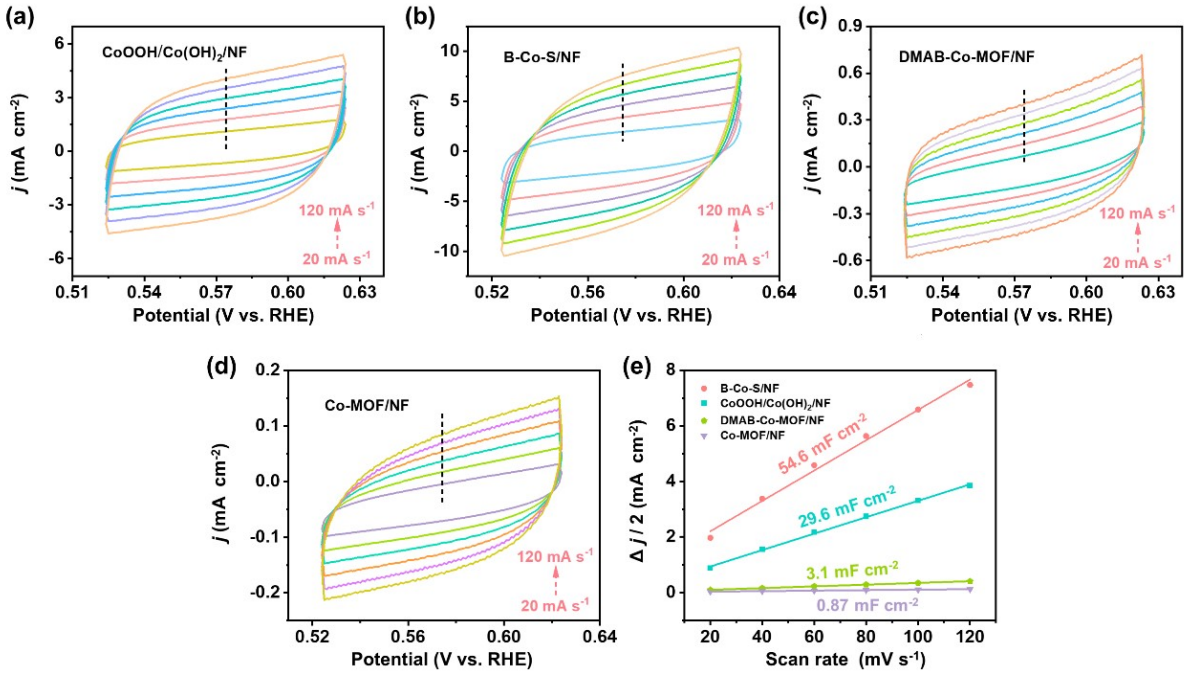

Fig. S14. CV curves of (a) $CoOOH/Co(OH)_2$/NF, (b) B-Co-S/NF, (c) DMAB-Co-MOF/NF and (d) Co-MOF/NF with various scan rates from 20 to 120 mV s^{-1}. (e) Plots of the current density versus the scan rate for $CoOOH/Co(OH)_2$/NF, B-Co-S/NF, DMAB-Co-MOF/NF and Co-MOF/NF with various scan rates from 20 to 120 mV s^{-1} at 0.574 V *vs.* RHE.

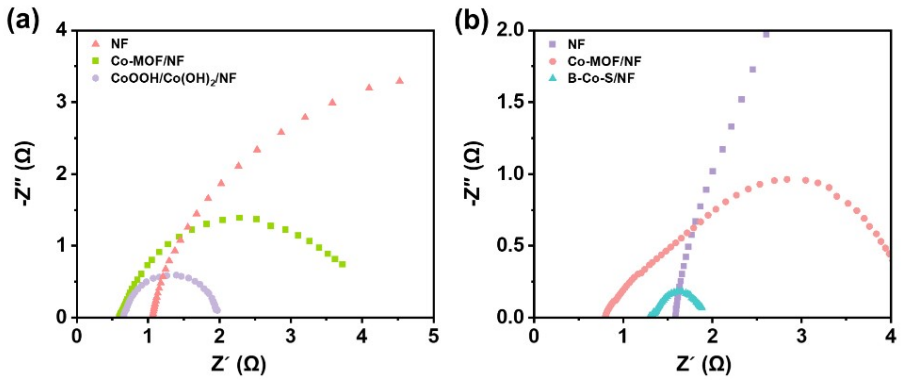

Fig. S15. EIS spectra of various catalysts in (a) 1 M KOH with 200 ppm KNO_3-N at -0.23 V *vs.* RHE and (b) 1 M KOH with 4 M Na_2S at 0.27 V *vs.* RHE.

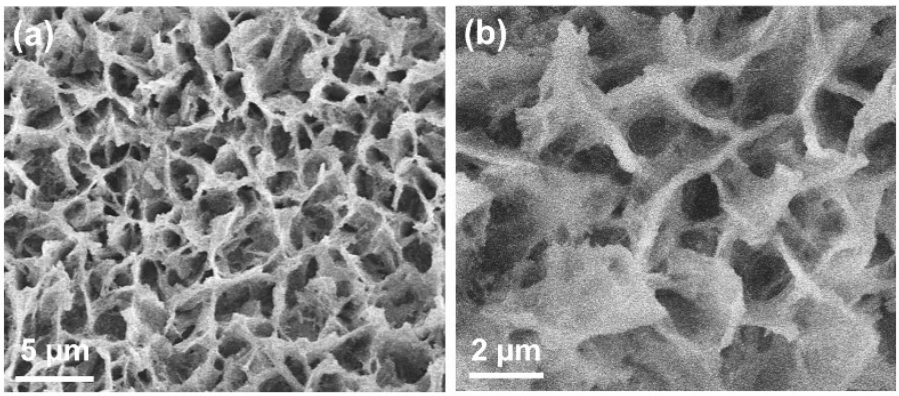

Fig. S16. SEM images of (a) $CoOOH/Co(OH)_2$/NF for NRA and (b) B-Co-S/NF for SOR after long-term stability testing.

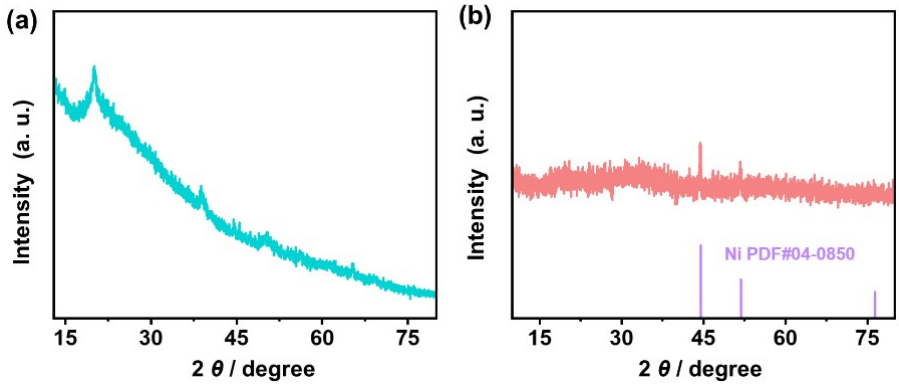

Fig. S17. XRD patterns of (a) $CoOOH/Co(OH)_2$/NF for NRA and (b) B-Co-S/NF for SOR after long-term stability testing.

Table S1. The NRA performance comparison between the $CoOOH/Co(OH)_2$/NF and some other reported electrocatalysts.

Electrocatalysts	Electrolytes	NH_3 FE	NH_3 yield rate	Ref.
$CoOOH/Co(OH)_2$/NF	**1 M KOH+ 200 ppm KNO_3-N**	**94.16%**	**0.238 mmol h^{-1} cm^{-2} at −0.2 V vs. RHE**	**This work**
Cu/Cu_2O	0.01 M KOH+0.5 M Na_2SO_4 + 100 mM NO_3^-	88.0 ± 1.6%	583.6 ± 2.4 μmol cm^{-2} h^{-1} at −1.0 V vs. RHE	1
PdMoCu	1 M KOH + 0.1 M KNO_3	56.95%	250.4 μmol h^{-1} cm^{-2} at −0.6 V vs. RHE	2
CoO@NCNT/GP	0.1 M NaOH + 0.1 M $NaNO_3$	93.8±1.5 %	9041.6±370.7 mg h^{-1} cm^{-2} at −0.6 V vs. RHE	3
Pd10Cu/BCN	0.1 M KOH + 100 mM NO_3^-	91.74%	102,153 μg h^{-1} mg_{cat}^{-1} at −0.6 V vs. RHE	4
CuCoSP	0.1 M KOH + 0.1 M NO_3^-	93.3 ± 2.1%	1.17 mmol h^{-1} cm^{-1} at −0.175 V vs. RHE	5
In-S-G	1 M KOH + 0.1 M KNO_3	75%	220 mmol h^{-1} $g_{cat.}^{-1}$ at −0.5 V vs. RHE	6
Ag/ZnO	1 M KOH + 0.1 M KNO_3	66%	516 mmol g_{cat}^{-1} h^{-1} at −0.6 V vs. RHE	7
$Bi\text{-}X_{red}$	1 M KOH + 0.5 M NO_3^-	90.6%	46.5 g h^{-1} g_{cat}^{-1} at −0.8 V vs. RHE	8
Cu-N-C SAC	0.1 M KOH + 0.1 M KNO_3	84.7%	4.5 mg cm^{-2} h^{-1} at −1 V vs. RHE	9
Cu_2O/Cu	1 M KOH + 250 mg L^{-1} NO_3^-	84.36%	2.17 mg cm^{-2} h^{-1} at −0.25 V vs. RHE	10

Table S2. The SOR performance comparison between the B-Co-S/NF and some other reported electrocatalysts.

Electrocatalysts	Electrolytes	Potential (V) at 100 mA cm^{-2}	Ref.
B-Co-S/NF	**1 M KOH+1 M Na_2S**	**0.380**	**This work**
	1 M KOH+4 M Na_2S	**0.268**	
CoS_2@C/MXene/NF	1 M NaOH+1 M Na_2S	0.389	[11]
NiSe/NF	1 M NaOH+1 M Na_2S	0.490	[12]
TPA@Ni_3S_2/NF	1 M NaOH+1 M Na_2S	0.480	[13]
CuCoS/CC	1 M NaOH+4 M Na_2S	~0.320	[14]
Cu_2S/NF	1 M NaOH+1 M Na_2S	0.440	[15]
CoNi@NGs	1 M NaOH+1 M Na_2S	0.520	[16]
Co-Ni_3S_2	1 M NaOH+1 M Na_2S	0.590	[17]
HEDP-Rh metallene	1 M KOH+4 M Na_2S	0.583	[18]

References

1. Y. Bu, C. Wang, W. Zhang, X. Yang, J. Ding and G. Gao, *Angew. Chem., Int. Ed.*, 2023, **62**, e202217337.
2. X. Tong, Z. Zhang, Z. Fang, J. Guo, Y. Zheng, X. Liang, R. Liu, L. Zhang and W. Chen, *J. Phys. Chem. C*, 2023, **127**, 5262-5270.
3. Q. Chen, J. Liang, L. Yue, Y. Luo, Q. Liu, N. Li, A. A. Alshehri, T. Li, H. Guo and X. Sun, *Chem. Commun.*, 2022, **58**, 5901-5904.
4. X. Zhao, X. Jia, H. Zhang, X. Zhou, X. Chen, H. Wang, X. Hu, J. Xu, Y. Zhou, H. Zhang and G. Hu, *J. Hazard. Mater.*, 2022, **434**, 128909.
5. W. He, J. Zhang, S. Dieckhofer, S. Varhade, A. C. Brix, A. Lielpetere, S. Seisel, J. R. C. Junqueira and W. Schuhmann, *Nat. Commun.*, 2022, **13**, 1129.
6. F. Lei, W. Xu, J. Yu, K. Li, J. Xie, P. Hao, G. Cui and B. Tang, *Chem. Eng. J*, 2021, **426**, 131317.
7. F. Lei, K. Li, M. Yang, J. Yu, M. Xu, Y. Zhang, J. Xie, P. Hao, G. Cui and B. Tang, *Inorg. Chem. Front.*, 2022, **9**, 2734-2740.
8. N. Zhang, J. Shang, X. Deng, L. Cai, R. Long, Y. Xiong and Y. Chai, *ACS Nano*, 2022, **16**, 4795-4804.
9. J. Yang, H. Qi, A. Li, X. Liu, X. Yang, S. Zhang, Q. Zhao, Q. Jiang, Y. Su, L. Zhang, J. F. Li, Z. Q. Tian, W. Liu, A. Wang and T. Zhang, *J. Am. Chem. Soc.*, 2022, **144**, 12062-12071.
10. W. Fu, Z. Hu, Y. Zheng, P. Su, Q. Zhang, Y. Jiao and M. Zhou, *Chem. Eng. J*, 2022, **433**, 133680.
11. L. Zhang, Z. Wang and J. Qiu, *Adv. Mater.*, 2022, **34**, e2109321.
12. C. Duan, C. Tang, S. Yu, L. Li, J. Li and Y. Zhou, *Appl. Catal. B: Environ.*, 2023, **324**, 122255.
13. L. Jin, C. Chen, L. Hu, X. Liu, Y. Ding, J. He, H. Li, N. Li, D. Chen, Q. Xu and J. Lu, *Applied Surface Science*, 2022, **605**, 154756.
14. H. Yu, W. Wang, Q. Mao, K. Deng, Y. Xu, Z. Wang, X. Li, H. Wang and L. Wang, *J. Mater. Chem. A*, 2023, **11**, 2218-2224.
15. Y. Pei, J. Cheng, H. Zhong, Z. Pi, Y. Zhao and F. Jin, *Green Chem.*, 2021, **23**, 6975-6983.
16. M. Zhang, J. Guan, Y. Tu, S. Chen, Y. Wang, S. Wang, L. Yu, C. Ma, D. Deng and X. Bao, *Energy Environ. Sci.*, 2020, **13**, 119-126.
17. Y. Li, Y. Duan, K. Zhang and W. Yu, *Chem. Eng. J*, 2022, **433**, 134472.
18. Z. Wang, G. Yang, P. Tian, X. Li, K. Deng, H. Yu, Y. Xu, H. Wang and L. Wang, *Chem. Eng. J*, 2023, **473**, 145147.